Application of Lidar to resolving tectonic and glacial fabrics in glaciated terrain: An example from an Archean granite-greenstone belt, northeastern Minnesota

Jonathan Dyess and Vicki L. Hansen
Department of Geological Sciences, University of Minnesota Duluth, 1114 Kirby Drive, 229 Heller Hall, Duluth, Minnesota 55812, USA

ABSTRACT

In this study we examine an Archean granite-greenstone terrane in northeastern Minnesota (USA) to illustrate the application of high-resolution Lidar (light detection and ranging) altimetry to mapping regional tectonic fabrics in forested glaciated areas. We describe the recognition of lineaments and distinguish between tectonic and glacial lineament fabrics. We use a 1-m Lidar derived bare earth digital elevation model to construct multiple shaded-relief images for lineament mapping with sun elevation of 45° and varying sun azimuth in 45° intervals. Two suites of lineaments are apparent. Suite A has a unimodal orientation, mean trend of 035, and consists of short (< 2 km long) lineaments within sediment deposits and bedrock. Suite B lineaments, which are longer (1–30 km) than those of suite A, have a quasi-bimodal orientation distribution, with maximum trends of 065 and 090. We interpret suite A as a surficial geomorphologic fabric related to glaciation, and suite B as a proxy for the regional tectonic fabric. Field measurements of regional tectonic foliation trajectories are largely consistent with suite B lineaments across the study area. Although not all suite B lineaments correlate to mapped structures, our analysis demonstrates that high-resolution Lidar altimetry can be useful in mapping regional tectonic fabrics in glaciated terrane.

INTRODUCTION

Regional tectonic fabrics commonly define the broad structural architecture of an area. Tectonic fabrics commonly have an associated topographic expression that may be identified via remote sensing (Chardon et al., 2002, 2008, 2009; Bedard et al., 2003). In glaciated terrains, vegetation, sediment cover, low overall topographic relief, and overprinting of glacial fabrics can variably obscure tectonic topographic expression and hinder identification via traditional remote sensing data sets such as satellite imagery and aerial photography. Therefore, mapping tectonic fabrics in glaciated terranes commonly does not lend itself to rapid remote sensing–based approaches. A remote sensing method for mapping regional tectonic fabrics within and across glaciated terranes could prove valuable in providing a regional structural framework, complimenting and expediting subsequent field mapping.

Airborne Lidar (light detection and ranging) systems provide high-resolution altimetry in vegetated areas (e.g., Haugerud et al., 2003). Widespread geoscience applications of airborne Lidar involve mapping of geomorphic features (typically beneath dense vegetative cover) including landslides, stream channels, alluvial fans, and fault scarps (e.g., Haugerud et al., 2003; Collins and Sitar, 2008; Roering, 2008; Notebaert et al., 2009). Applications of Lidar altimetry in structural geology include identifying structural fabrics via analysis of (1) morphometric features (e.g., slope, aspect, and curvature) (Wallace et al., 2006) and (2) microtopography (e.g., Pavlis and Bruhn, 2011). However, the use of Lidar altimetry to map regional tectonic fabrics in continentally glaciated terrain remains unexplored.

In this contribution we examine a portion of an Archean granite-greenstone terrane in northeastern Minnesota (USA) and illustrate the application of high-resolution Lidar altimetry to mapping regional tectonic fabrics in forested, continentally glaciated regions. We discuss lineament recognition using Lidar and distinguish between tectonic and glacial lineament fabrics. We also discuss potential applications and Lidar data limitations.

GEOLOGIC SETTING

The study area is within the Vermilion District granite-greenstone terrane of northeastern Minnesota (Fig. 1). The Vermillion district includes, from north to south, the Vermillion Granitic Complex, various greenschist facies metavolcanic and metasedimentary sequences, and the quartz monzonite Giant's Range batholith (Sims, 1976). Granite, granite-rich and biotite-rich migmatites, biotite and amphibolite schists, metagabbro, metabasalt, and trondhjemite characterize the Vermilion Granitic Complex. Greenschist facies metavolcanic and metasedimentary sequences, which include protoliths of basalt, diabase, pyroxenite, basalt flows, felsic to intermediate volcanic tuff, felsic volcanic rocks, conglomerate, graywacke, shale, and banded iron formation, are cut by ovoid granitoid bodies (Sims, 1976). Volcanic and plutonic rocks range in age from 2.75 to 2.69 Ga and from 2.74 to 2.65 Ga, respectively (Card, 1990, and references therein). Paleoproterozoic plutonic rocks intrude along the southeastern margin of the study area (Gruner, 1941; Jirsa and Miller, 2004).

The Vermillion district volcano-sedimentary sequence hosts several east-northeast–striking subvertical ductile shear zones. These shear zones extend up to ~70 km long and 7–10 km wide, although shear zone boundaries are diffuse. An anastomosing metamorphic foliation is present across the shear zones with an average orientation of 065, 90 (Bauer and Bidwell, 1990; Erickson, 2008, 2010; Wolf, 2006; Goodman, 2008). Layering, where notable, is parallel to local foliation. Narrow areas of well-developed C-foliation mark high-strain zones typically parallel to the regional foliation (Bauer and Bidwell, 1990; Wolf, 2006). High-strain zones have been recognized locally within an individual shear zone and may exist throughout the various zones; however, the extent of these high-strain zones remains unconstrained (Bauer and Bidwell, 1990; Wolf, 2006). High-strain zones, ~1.5 km apart, are postulated to accommodate significant deformation relative to areas containing only the regional foliation.

The study area is part of the Superior Uplands geomorphic province, a glacially scoured

Geosphere; October 2014; v. 10; no. 5; p. 987–997; doi:10.1130/GES00984.1; 11 figures; 1 table.
Received 24 September 2013 ♦ Revision received 12 June 2014 ♦ Accepted 7 August 2014 ♦ Published online 29 August 2014

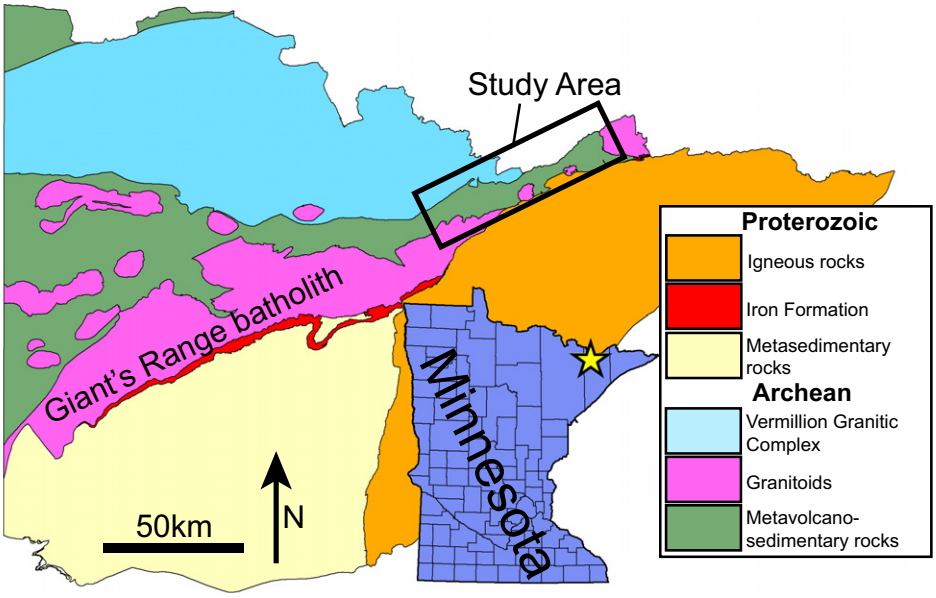

Figure 1. Simplified geologic map of northeastern Minnesota (USA). Rectangle indicates location of Figure 2.

peneplain characterized by level terrain to rolling uplands and hills (McNab and Avers, 1994). Dense coniferous and deciduous forests cover the study area, in addition to numerous swampy areas and lakes. Glacially scoured bedrock with areas of thin till or other sediments dominates the surficial geology of the study area. Glacial geomorphologic features include flutes, drumlins, and eskers (Hobbs and Goebel, 1982; Sharp, 1953).

DATA AQUISITION

In 2011 Lidar altimetry data were collected over the study area as part of the Minnesota Elevation Mapping Program (Fig. 2). Data were collected during leaf-off conditions to maximize beam penetration. Full data acquisition details are provided in Table 1. The principle products of the Lidar survey were classified LAS (Log ASCII Standard) formatted point cloud data, a 1 m digital elevation model (DEM), and edge of water breaklines. Secondary products produced by the Minnesota Department of Natural Resources include 2 ft (~0.6 m) topographic contours and building outlines. The Lidar-derived 1 m filtered bare earth DEM, based on last return data, is the primary raw data set for this study. A pixel resolution of 1 m coupled with sub-meter vertical accuracy allowed for the detection of relatively small scale topographic features.

LIDAR AS A FIELD MAPPING TOOL

In order to determine an efficient way to recognize linear features, we analyzed the raw data in three different forms using ESRI ArcGIS software. We analyzed the original bare earth DEM and Lidar-derived shaded-relief images, and draped the shaded relief images over the DEM to create three-dimensional (3D) perspective views of the field area. Linear ridges, valleys, shorelines, islands, or elongate ellipsoidal hills define topographic lineaments; we map lineaments by tracing these features or associated long axes. Due to the subvertical nature of the regional structural architecture of the study area, certain lineaments may represent structural trends. This analysis would be inappropriate for areas dominated by gently dipping structures.

Lineament mapping is an iterative process and need not be completed in the sequence described in the following. Lineament identification was done manually, and in order to recognize lineaments within a given area, it is best to repeatedly analyze areas using all available forms of the data. Lineament mapping was conducted at multiple scales, ranging from regional (~1:250,000) to a single DEM tile (~1:24,000). The goal of this analysis was to identify lineaments of any orientation and observe what patterns or subsets naturally emerged (lineament mapping for this study was carried out by Dyess).

We initially created a single DEM mosaic covering the entire study area; however, due to the large size of the study area and high resolution of the data, we opted to create three smaller mosaics in order to reduce file size and processing time. We applied a stretched color ramp to the data utilizing both grayscale and full color symbolization. Full color revealed more linear features than grayscale. Within the DEM visible lineaments commonly correspond with shorelines, cliffs, and ridges (Fig. 3A). Pronounced lineaments correspond to features with relatively high topographic relief; however, subtle topographic features are obscured and many small-scale lineaments are not easily visible in the DEM (Fig. 3A).

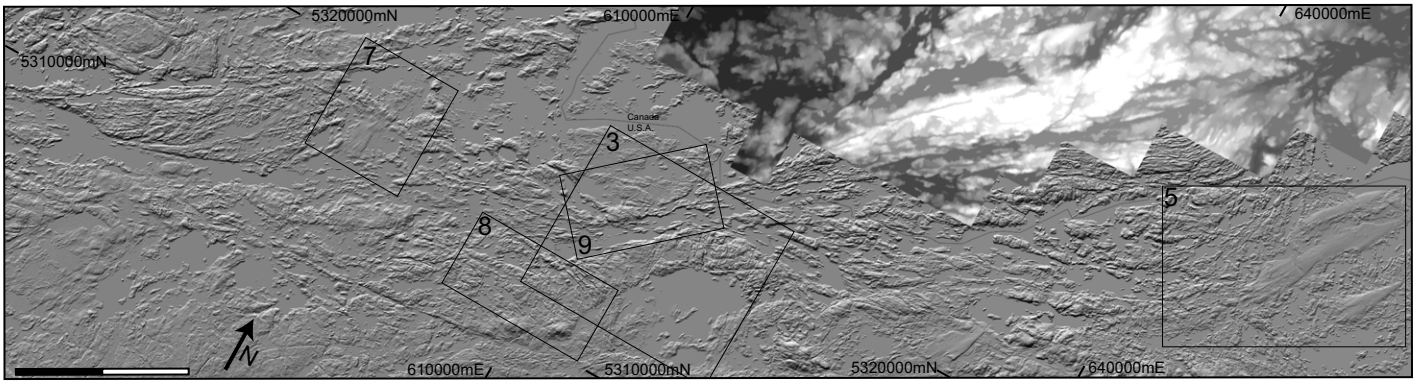

Figure 2. 1 m shaded-relief image of the study area. Rectangles indicate locations of Figures 3, 5, 7, 8, and 9; 15 m digital elevation model of Ontario is included for completeness. Location of Figure 2 given in Figure 1. Coordinate system UTM Zone 15, NAD 1983.

TABLE 1. LIGHT DETECTION AND RANGING DATA ACQUISITION DETAILS

Project vendor	Woolpert, Inc.
Flight altitude (above terrain)	1982.2 m
Post spacing	1 m
Average ground speed	66 m/s
Pulse rate	115.6 kHz
Scan rate	41.8 kHz
Field of view	40°
Side lap (minimum)	25%
Swath width	variable
Distance between flight lines	variable
Horizontal accuracy	1 m
Vertical accuracy RMSE	5 cm
Coordinate system	UTM Zone 15
Horizontal datum	NAD83
Vertical datum	NAVD88 Geoid09
Horizontal unit	m

Note: Data available at ftp://ftp.lmic.state.mn.us/pub/data/elevation/lidar. RMSE—root mean square error; UTM—Universal Transverse Mercator; NAD—North American Datum; NAVD—North American Vertical Datum.

We constructed shaded-relief images from the original DEM (Fig. 3B). A shaded-relief image is a raster image showing changes in elevation using light and shadows on terrain based on a given sun azimuth and sun elevation (Zhou, 1992). Sun azimuth and sun elevation are critical to lineament mapping using shaded-relief images. Shaded-relief images may be created for any sun azimuth or sun elevation, even unnatural sun azimuths, which may reveal subtle topographic features not visible in the bare earth DEM (Henderson et al., 1996; Pavlis and Bruhn, 2011). Lineaments that trend perpendicular to the sun azimuth are easily visible, whereas lineaments that trend parallel to the sun azimuth are obscured (Fig. 4). Relatively small lineaments that trend parallel to the sun azimuth were commonly obscured to the point of being invisible, and the recognition of relatively large lineaments in this same trend was greatly reduced. In order to recognize all orientations of lineaments, we constructed shaded relief images for sun azimuths that varied from 315 to 090 at 45° increments (Fig. 4). We examined shaded-relief images with both equalized and unequalized histogram symbolization. Images with equalized histogram symbolization emphasize relatively large scale lineaments. Relatively small lineaments within topographically high areas were commonly obscured by highlights within the image. Images with unequalized histogram symbolization commonly captured small-scale lineaments.

In order to better visualize the topographic surface in 3D, we draped shaded relief images over the bare earth DEM using ESRI ArcScene to create a 3D-perspective view (e.g., Pavlis and Bruhn, 2011). Due to the overall low topographic relief across the study area, we applied both 5× and 10× vertical exaggeration to the DEM. Within these oblique views, lineaments appear pronounced with vertical edges; however, vertical faces hide structural elements. Surficial features are easily visible within these oblique views.

SURFACE COVER TYPES

Visible within the shaded-relief images are two surface cover types, each with a distinctive Lidar signal (Fig. 5). Cover types were recognized and mapped during the lineament-mapping process. Cover type I (CTI) comprises the vast majority of study area and occurs as bulbous, irregular topographic surface containing various linear and irregular shaped features. Cover type II (CTII) occurs in elongate patches across the study area and contains relatively smooth topography compared to CTI. Boundaries between CTI and CTII vary from sharp to gradational. At gradational boundaries, topographic features consistent with CTI are visible beneath CTII, indicating that CTII overlies CTI. This relationship is consistent across the study area. Ground truthing indicates that CTI correlates to areas of scoured bedrock. Long-axis orientations of CTII patches are consistent with long-axis orientations of drumlins (Hobbs and Goebel, 1982); therefore we interpret CTII as areas of glacial sediment cover.

LINEAMENT SUITES

Lineament fabrics visible within Lidar altimetry are inherently geomorphic fabrics. Both preexisting bedrock structure and erosion processes effect the formation of geomorphic linear features. Lineaments may be surficial (i.e., dominantly controlled by erosion processes) or structural (i.e., dominantly bedrock controlled). Both surficial and structural lineaments are geomorphic features; however, surficial lineaments need not reflect the underlying bedrock geologic structure. Structural lineaments may represent the surface expression of a host of planar geologic structures, including bedding, faults, frac-

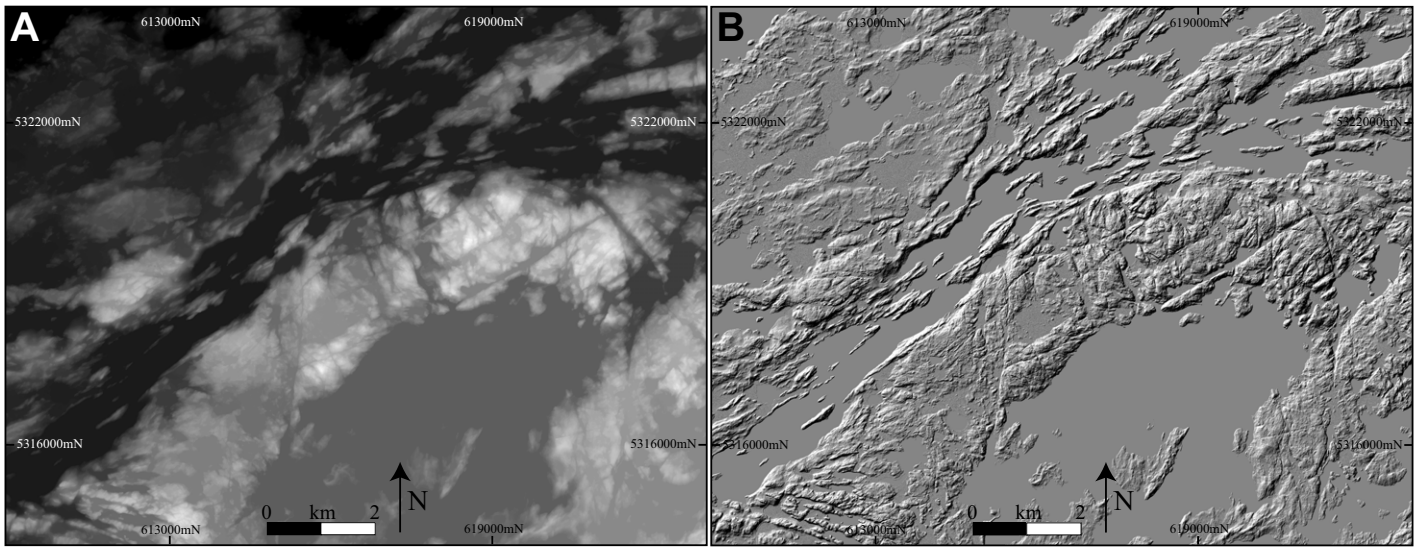

Figure 3. (A) Raw 1 m digital elevation model in grayscale showing a relatively fuzzy lineament fabric. Although large-scale lineaments are visible, relatively small-scale lineaments are not easily visible. (B) Lidar (light detection and ranging) derived shaded-relief image showing a distinct lineament fabric with both large-scale and small-scale lineaments easily visible. Sun elevation is 45° and sun azimuth is 315. Coordinate system UTM Zone 15, NAD 1983.

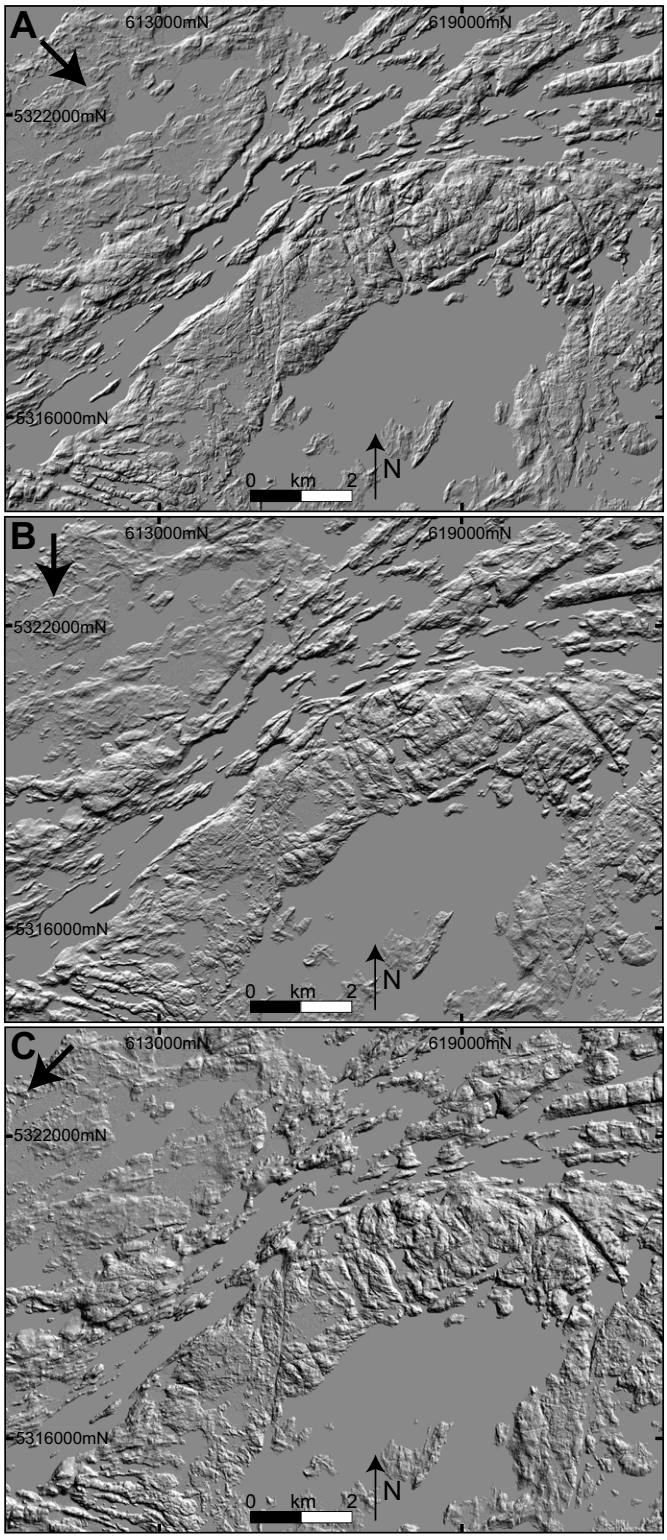

Figure 4. Shaded-relief images constructed with a sun elevation of 45° and varying sun azimuth (large arrows indicate direction). (A) Sun azimuth 315. (B) Sun azimuth 000. (C) Sun azimuth 045. Lineaments trending perpendicular to sun azimuth are easily visible, whereas lineaments trending parallel to sun azimuth appear obscured or are invisible. Coordinate system UTM Zone 15, NAD 1983.

tures, foliation, or cleavage. Based on lineament shape characteristics, we classify lineaments into different suites and interpret these suites as either surficial or structural. By extracting structural lineaments, we delineate the structural fabric, which can provide insight into the geologic history of the area.

We recognize two distinct lineament suites. We base lineament classification on length, spacing, orientation, regional pattern, and the type of topographic feature defining the lineament. Classification considers all criteria rather than emphasizing an individual criterion. Lineament spacing was calculated by measuring intersection points along transects across representative areas. Both lineament mapping and lineament classification are iterative processes, the best result emerging after multiple cycles of mapping and classification.

Lineament suite A (Fig. 6A) consists of a series of straight, short, parallel lineaments commonly located within topographically high areas. Elongate rounded hills and narrow elongate valleys define suite A lineaments and range from 50 to >100 m across and 0.02 to 2.5 km long. Suite A lineaments have variable spacing (ranging from ~0.1 to 2 km) and unimodal orientation distribution with a mean trend of 035 (Fig. 6A). Areas of sediment cover contain only suite A lineaments at increasingly smaller scales (Fig. 7). Suite A lineaments are most visible within sediment cover with the shortest lineaments having lengths of 20 m. A set of narrow curvilinear features occurs within suite A (Fig. 6A). These features can be as long as 3.5 km and approximately parallel the dominant trend of suite A lineaments (Fig. 6A).

Lineament suite B forms a pattern of roughly parallel continuous curvilinear features that commonly bound topographically high areas and have varying trend (Fig. 6B). Curvilinear shorelines, cliffs, ridges, valleys, and elongate islands define suite B lineaments, and range in length from <1 to 33 km. Linear features may extend for tens of kilometers as a single lineament, or occur as a series of short parallel segments. Suite B lineament trends range from 000 to 110 and show a weakly bimodal orientation distribution with a dominate trend of 065, and a subsidiary trend of 090 (Fig. 6B). The suite B lineament fabric includes domains of pervasive parallel lineaments, spaced parallel lineaments, and spaced lineaments with no apparent preferred orientation.

In regions where suite A and B lineaments occur at high angles, a distinctive interference pattern results (Fig. 8). In a shaded-relief image with suite A and suite B lineament fabrics and the corresponding lineament map, suite A lineaments grade from well-developed

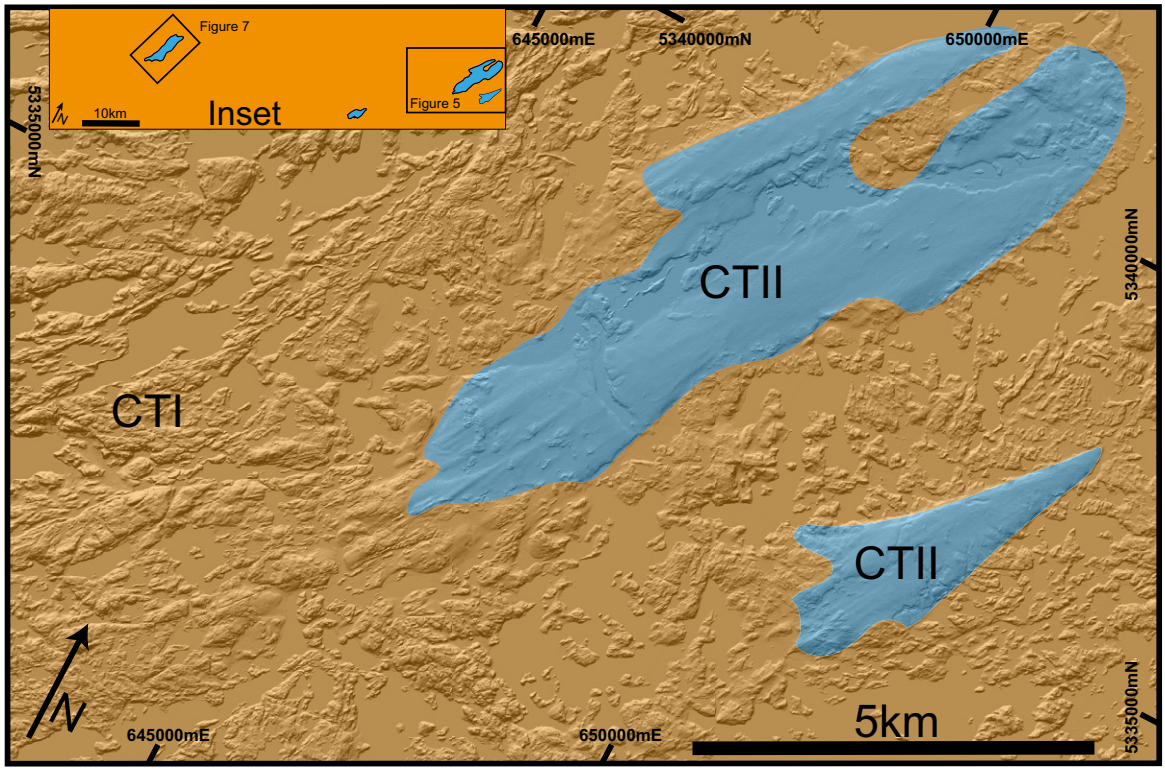

Figure 5. Map showing surface cover types (CTI and CTII) and corresponding Lidar (light detection and ranging) shaded-relief image. CTI (orange) corresponds to scoured bedrock. CTII (blue) corresponds to sediment cover. Inset: Cover-type map of the entire study area (area of Fig. 2) showing extent of sediment cover. Rectangles mark the locations of Figures 5 and 7. Coordinate system UTM Zone 15, NAD 1983.

in the west to poorly developed to nonexistent in the east. Although suite A lineaments do not occur ubiquitously across the area, suite A lineaments consistently define a parallel fabric within topographically high areas. Conversely, suite B lineaments commonly bound topographically high areas and define a relatively spaced fabric. Where both lineament suites trend at relatively high angles to one another, suite A lineaments occur in topographically high areas between individual suite B lineaments (Fig. 8).

Where suite A and B lineaments trend parallel to one another, differentiating the lineament sets is difficult. Figure 9 shows a shaded relief image and corresponding lineament map; here suite B lineaments trend 050 and a set of nearby suite A lineaments trend 045. Along the southeast margin of the image, a single pervasive lineament set trends 050. These lineaments are classified as suite B due to topographic expression and length. However, given that suite A and B lineaments are nearly parallel, it is likely that some suite A lineaments occur within areas dominated by suite B lineaments (Fig. 9). Along the northwest edge of the image, the angle between suites A and B is 35°, resulting in an interference pattern of relatively pervasive suite A lineaments between relatively spaced suite B lineaments.

INTERPRETATION OF LINEAMENT FABRICS

We interpret suite A lineaments as reflecting topographic features related to glaciation. Suite A lineaments appear in both areas of sediment cover and exposed bedrock; however, areas with interpreted lineated sediment cover contain only suite A lineaments, and lineaments are continuous across the sediment-bedrock interface (Fig. 7). Suite A lineaments commonly parallel mapped glacial flutes and drumlins (Hobbs and Goebel, 1982) (Fig. 6A). We interpret the narrow sinus ridges as eskers; these features trend roughly parallel to suite A lineaments. Suite A lineaments are relatively consistent in length, spacing, and orientation across the study area regardless of the underlying bedrock geologic structure. This relationship implies that bedrock geologic structure is not the dominant control on suite A lineament orientation. We interpret suite A lineaments as a surficial geomorphic fabric controlled dominantly by glaciation and erosion.

Suite A lineaments do not always parallel glacial features recognized in the field. For example, in Figure 6A, glacial flutes trend 055 and 060 at locations iii and iv, respectively (Hobbs and Goebel, 1982), whereas suite A lineaments trend 025; at locations iii and iv the lineaments are relatively long and continuous, and correspond to topographic features with relatively high relief compared to typical suite A lineaments. We interpret these lineaments as suite B lineaments accentuated by glaciation.

Suite B lineaments commonly correlate with structural trajectories of bedrock tectonic fabric (Fig. 10) (Bauer and Bidwell, 1990; Goodman, 2008; Erickson, 2010; Mulvey, 2009; Jirsa et al., 2011). Structures parallel to suite B lineaments include bedding, metamorphic foliation, and faults; however, some parts of the suite B lineament fabric may correlate well with structural trajectories. We divide the suite B lineament fabric into domains based on lineament orientation and density for illustrative purposes only (Fig. 10A); domain boundaries are approximate with no apparent geologic significance. Figure 10 shows a portion of the suite B lineament fabric and the corresponding structural trajectories. Closely spaced, pervasive, parallel suite B lin-

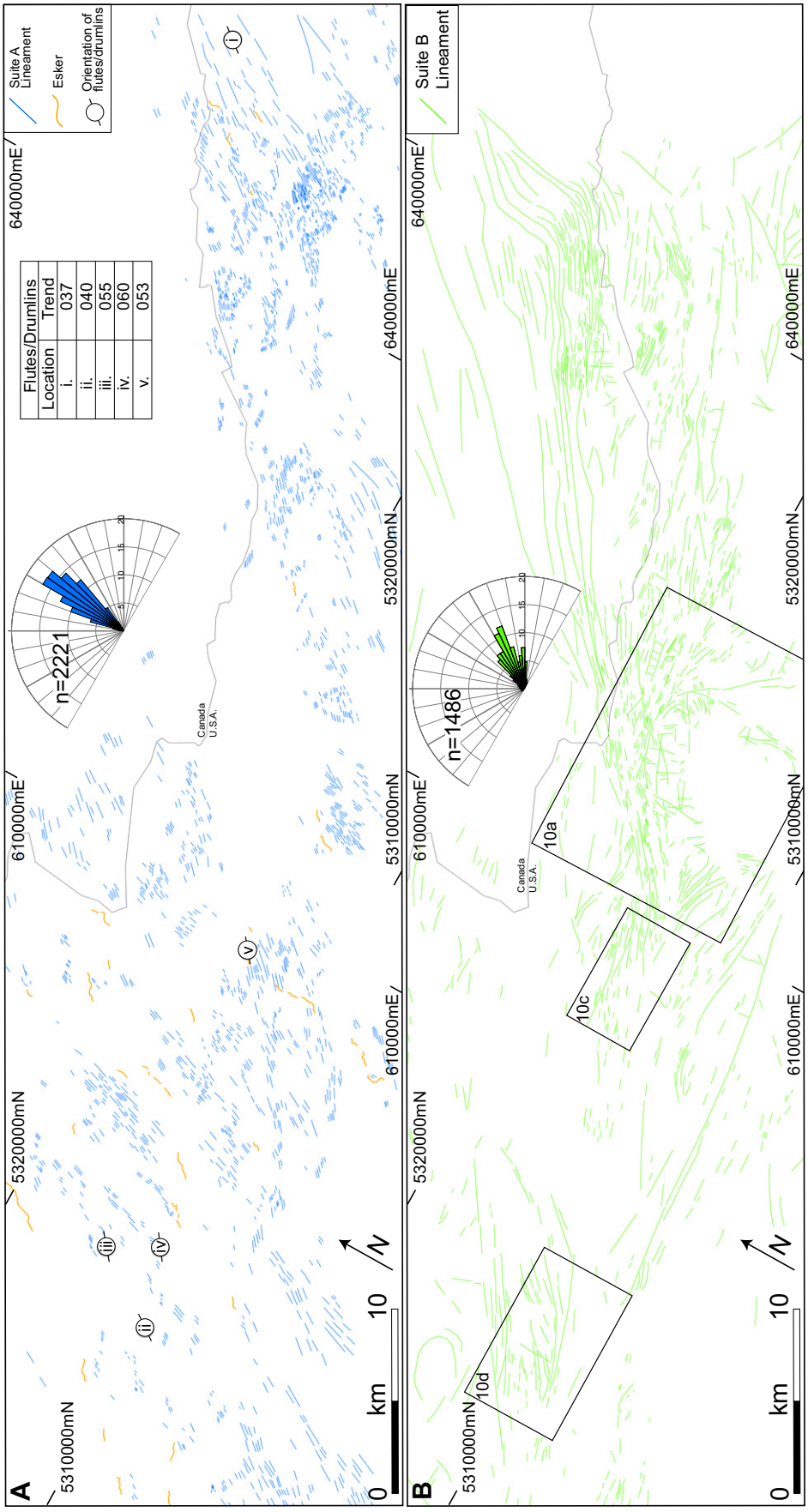

Figure 6. (A) Map showing the complete suite A lineament fabric and corresponding rose diagram. Center inset: i–v mark the locations and orientations of glacial flutes and/or drumlins mapped by Hobbs and Goebel (1982). (B) Map showing complete suite B lineament fabric and corresponding rose diagram. Rose diagram radial axes are labeled in percent of total data points; diagrams display average trend of each lineament. Locations of Figure 10 are shown. Coordinate system UTM Zone 15, NAD 1983.

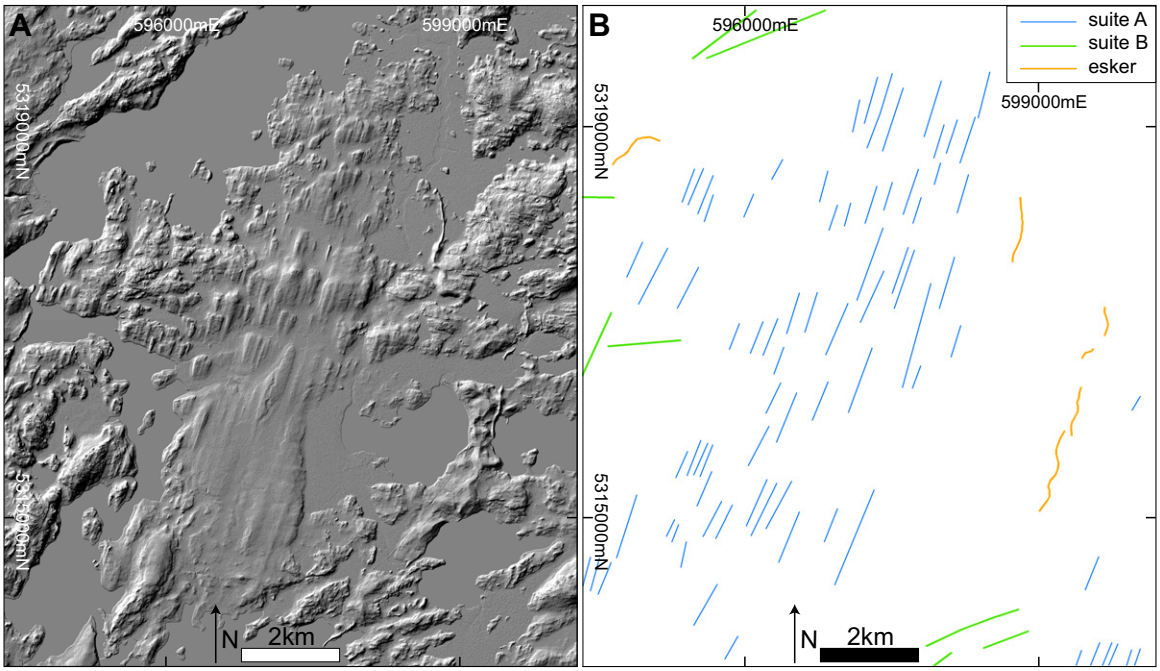

Figure 7. (A) 1 m Lidar (light detection and ranging) derived shaded-relief image showing the topographic expression of various linear features within areas of scoured bedrock and shallow sediment cover. (B) The corresponding lineament map. Sun azimuth is 315 and sun elevation is 45°. Coordinate system UTM Zone 15, NAD 1983.

eaments mark domains U, V, and W and correlate well with bedding, metamorphic foliation, and fault trajectories collectively. The dominant structural trend in domain U is 065; lineaments trend east and southeast in domains V and W, respectively.

Domain X is largely devoid of lineaments; in this region, conglomerate, sandstone, and shale dominate the local geology, and primary structures (sedimentary bedding) are prevalent, whereas mapped secondary structures (i.e., faults and metamorphic foliation) are rare to nonexistent (Fig. 10B) (Mulvey et al., 2009). This inverse correlation between suite B lineaments and bedding trajectory implies that bedding orientation has little effect on suite B lineament orientation, at least at this location. Spaced lineaments characterize domain Y, which also records few secondary structures.

Intersecting lineaments with no apparent preferred orientation characterize domain Z (Fig. 10A). These lineaments show no correlation with previously recognized primary or secondary structures; however, it is possible that other secondary structures (e.g., fractures) control suite B lineament orientation within domain Z. Due to the close correlation between parallel suite B lineaments and secondary structural trajectories, we interpret areas of parallel suite B lineaments as representing the secondary structural (tectonic) fabric across the study area. We recognize a correlation between parallel suite B lineaments and secondary structures in nearby areas as well (Figs. 10C, 10D).

NEW VIEW OF THE REGIONAL TECTONIC FABRIC

Using suite B lineament fabric in conjunction with field data, we interpret the tectonic fabric across the study area and present a 2D representation of the regional tectonic fabric (Fig. 11). The lack of 3D information is a function of the overall low topographic relief and the dominant subvertical orientation of geologic structures. The regional tectonic fabric represents a structural continuum with gradational variation in orientation and density. Although individual lineaments do not correspond one-for-one with individual structures, the patterns within the lineament fabric track regional foliation trajectory and allow for first-order observations. The regional tectonic fabric is dominantly within and parallel to metavolcanic-metasedimentary sequence boundaries. We distinguish three types of areas within the tectonic fabric: pervasive parallel fabric, spaced parallel fabric, and intersecting fabric. Regions of pervasive parallel fabric form a curvilinear zone across the study area and, based on field observations, correspond with areas of well-developed metamorphic foliation and faults (Fig. 11). Regions of spaced parallel fabric correspond with weakly developed metamorphic foliation and a small number of faults, whereas areas of intersecting lineaments do not correspond to any recognized structures, although field access to this area is limited. We interpret areas of pervasive parallel tectonic fabric to represent the extent of shear zones within the metavolcanic-metasedimentary sequence, and areas of spaced lineaments to represent massive to weakly deformed rock.

Interaction of the tectonic fabric with granitoid bodies has implications for the relative timing between deformation and granitoid emplacement. The tectonic fabric is parallel to granitoid boundaries, and excluding the Giant's Range batholith, granitoids are largely devoid of any tectonic fabric (Fig. 11). Tectonic fabric commonly diverges around ovoid granitoids, such as around the Snowbank Lake stock, and near the Saganaga tonalite, particularly along the western margin (Fig. 11). One interpretation is that granitoids were at least partially emplaced and rheologically strong before formation of the tectonic fabric and that these bodies did not accommodate much (if any) deformation. Alternatively, granitoid emplacement could postdate formation of the tectonic fabric and simply reorient the tectonic fabric. Tectonic fabric appears continuous across the northern margin of the Giant's Range batholith and fades to the south, suggesting that the northern edge of the Giant's Range batholith

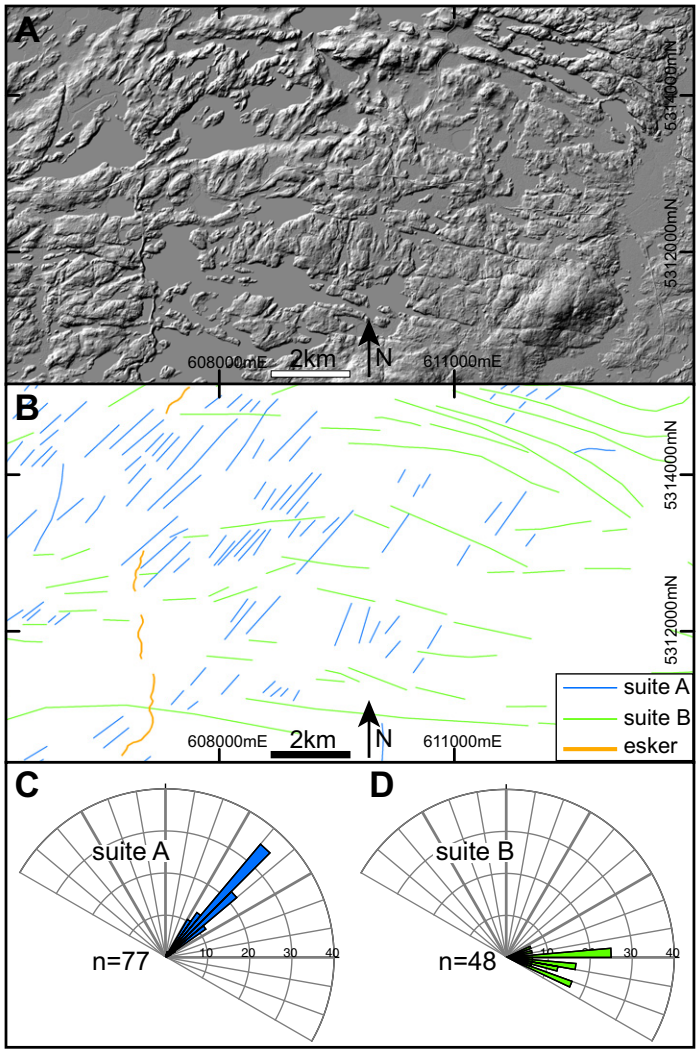

Figure 8. (A) Lidar (light detection and ranging) derived shaded-relief image. (B) The corresponding lineament map showing a localized lineament fabric with suite A and suite B lineaments at high angles to one another. (C) Rose diagram illustrates the local orientation distribution of suite A lineaments; diagram displays average trend of each lineament. Radial axes are marked in percent of total data points. (D) Suite B lineaments. Coordinate system UTM Zone 15, NAD 1983.

underwent some amount of solid-state deformation (Fig. 11). These differences may be due to the relatively large size of the Giant's Range batholith compared to the Saganaga tonalite and the Snowbank stock (Fig. 1).

FACTORS LIMITING RECOGNITION OF TECTONIC FABRIC IN GLACIATED TERRANE

Lidar shaded-relief images provide a spectacular view of the study area despite ubiquitous vegetative cover. These data provide substantial improvements over aerial photographs and satellite imagery in recognizing bedrock structure. Lidar shaded-relief images clearly show areas of scoured bedrock and glacial sediment deposits. Sediment cover significantly limits the usefulness of this analysis. All lineaments interpreted as related to tectonic fabric occur within areas of glacially scoured bedrock with effectively no sediment cover. Significantly large and/or thick glacial deposits will completely obscure the tectonic fabric.

Topographic expression of the tectonic fabric is a function of lithology, geologic structure, and erosion processes. Although Lidar altimetry records high-resolution topography that may reflect changes in lithology or geologic structures, the rock's ability to form relatively small scale topography (microtopography) is critical. Microtopography is the product of relatively delicate water and wind erosion processes that are sensitive to subtle lithologic and/or structural changes (e.g., Pavlis and Bruhn, 2011). Bedrock in the study area underwent glacial scouring and frost wedging; such erosion processes destroy microtopography and result in a relatively coarse topographic surface.

Detailed Lidar mapping is difficult due to the relatively coarse topography; however, regional structural trends and structural zones emerge from the data. For a structural zone to be visible in the Lidar shaded-relief image, the zone must be large (wide) enough for the rock to preserve a distinct lineament fabric. Relatively narrow structural zones may appear as a single lineament or not at all. In addition, if a narrow structural zone (defined by a single lineament) is subparallel to the surficial glacial lineament fabric, distinguishing the nonglacial lineament from the glacial lineament fabric is difficult to impossible. At the outset of this analysis, two major goals were to use Lidar altimetry to distinguish structural relationships between the tectonic fabric and granitoids and to identify and map high-strain zones (e.g., Bauer and Bidwell, 1990; Wolf, 2006). Although some structural relationships between the tectonic fabric and individual granitoids are visible, identification of relatively narrow high-strain zones is difficult.

SUGGESTED METHODS FOR LINEAMENT MAPPING AND INTERPRETATION

First and foremost, lineament mapping is an iterative process. In this study, lineament identification was done manually, and no single image (e.g., DEM, shaded-relief) effectively captured all lineaments within a given area. Repeated mapping using as many images and symbologies as possible yielded the best results. Although no single method applies perfectly to every study area, we outline a suggested mapping method for recognizing lineaments at any orientation.

Depending on the size of the study area, mosaics of individual DEM tiles may be required. Because various shaded-relief images might be constructed and compared, creating a mosaic of the original Lidar DEM is perhaps most time efficient; however, the need for mosaics is dependent on computer processing power and software. For this study, dividing the study area into smaller mosaic subsets reduced

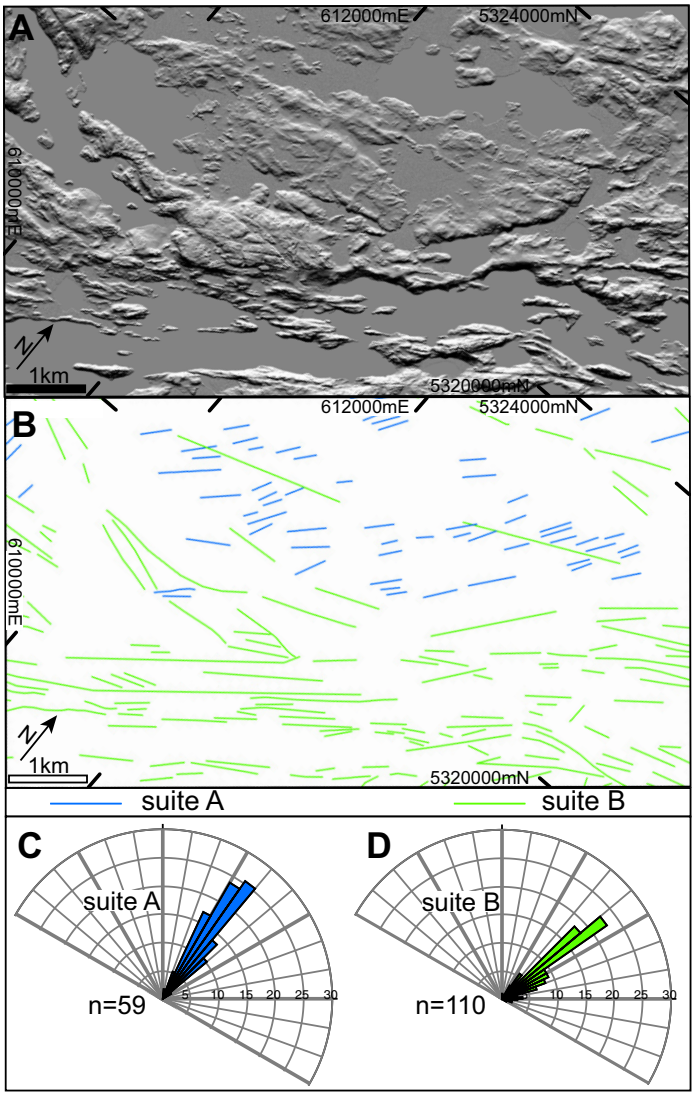

Figure 9. (A) Lidar (light detection and ranging) derived shaded-relief image. Note north direction. (B) The corresponding lineament map showing a localized lineament fabric with parallel suite A and suite B lineaments. (C) Rose diagram illustrates the local orientation distribution of suite A lineaments; diagram displays average trend of each lineament. Radial axes are marked in percent of total data points. (D) Suite B lineaments. Coordinates syste UTM Zone 15, NAD 1983.

individual file size and decreased the required processing power and time. Future studies using different software or enhanced computing power may not require this step.

Lidar shaded-relief images provide an efficient means of lineament recognition. Because lineament mapping requires many different shaded-relief images, careful attention to data processing is critical. Lineaments perpendicular to sun azimuth are most visible, whereas lineaments parallel to sun azimuth appear obscured. We found that creating multiple shaded-relief images by varying sun azimuth in 45° increments with a sun elevation of 45° to be a good starting point. After some initial mapping, other shaded-relief images may be created to investigate specific areas and lineament patterns. Examination of both equalized and nonequalized histogram shaded-relief images is useful. Equalized histogram symbolization highlights relatively large scale lineaments, whereas nonequalized histogram symbolization highlights relatively small-scale lineaments. Mapping in ESRI Arcmap or similar geographic information system software, accommodates this mapping method quite well because the original DEM and all subsequent shaded-relief images are georeferenced and can be overlain easily. Shaded-relief images with different sun azimuths can be turned on or off during mapping, quickly providing multiple views of a study area.

Lineament interpretation as either surficial or structural is nontrivial, especially if field observations are lacking. Identifying lineaments within known glacial features such as drumlins or glacial sediment can be used to distinguish between surficial and structural lineament suites within bedrock. Lineament orientation, spacing, and length are also critical to lineament interpretation. To achieve the best interpretation, we suggest a feedback loop between lineament mapping and comparison with field observations.

Interpretation of nonglacial lineaments depends largely on the regional geology and structural style of the study area. For this study metamorphic foliation and fault trajectories define the tectonic fabric. Areas of relatively pervasive parallel fabric correlate best with areas of well-developed foliation and faults. In other areas the relationship between the nonglacial lineament fabric and tectonic fabric could be quite different. Careful comparison of field observations and mapped lineaments is critical to making informed interpretations.

SUMMARY

High-resolution Lidar altimetry has potential for mapping lineaments related to both glacial geomorphological fabrics and regional tectonic fabrics related to bedrock structural geology. Our analysis shows that application of Lidar shaded-relief images of glaciated terrane has several applications in structural geology including (1) constructing preliminary regional tectonic fabric maps from limited field observations, allowing for the formation and testing of structural models; (2) directing field work to areas of interest to test structural models, making field work more efficient and decreasing field time; (3) providing insight into inaccessible areas or areas of poor exposure; (4) illustrating primary crosscutting relationships and relative timings; and (5) placing detailed map areas into a broad regional structural context.

Application of Lidar to this study area provides a 2D map view of the tectonic fabric. The lack of 3D information is a function of the overall low topographic relief and the dominant subvertical orientation of geologic structures. This 2D view limits the usefulness of this analysis and illustrates the need for field mapping to better understand the 3D structural setting.

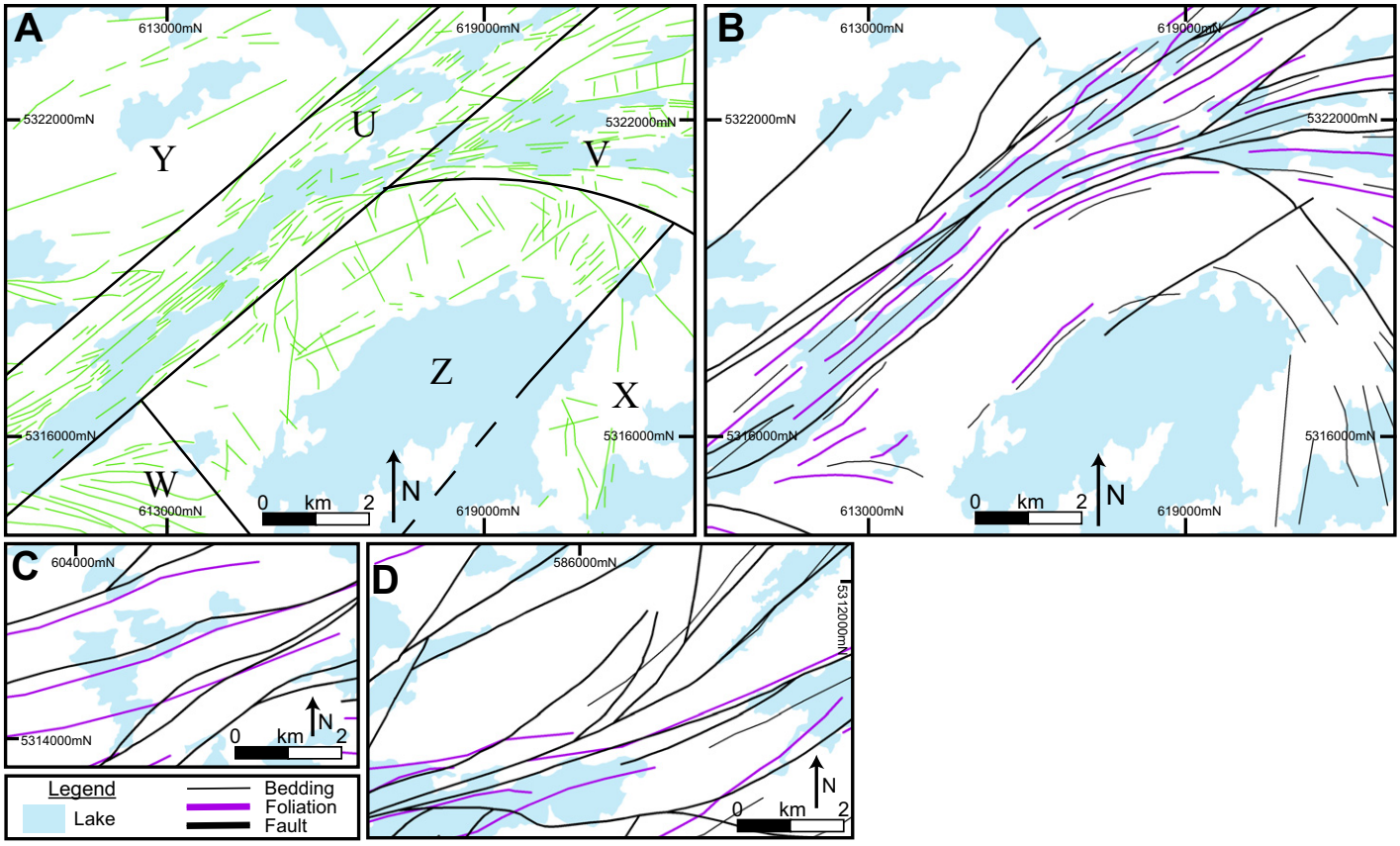

Figure 10. (A) Map showing localized suite B lineament fabric divided into six domains. (B) The corresponding structural trajectories. Domains are for illustrative purposes only. (C, D) Other selected areas showing structural trajectories (see Fig. 6 for map locations). Structural data are from Goodman (2008), Erickson (2008), Mulvey et al. (2009), and Jirsa et al. (2011). Coordinate system UTM Zone 15, NAD 1983.

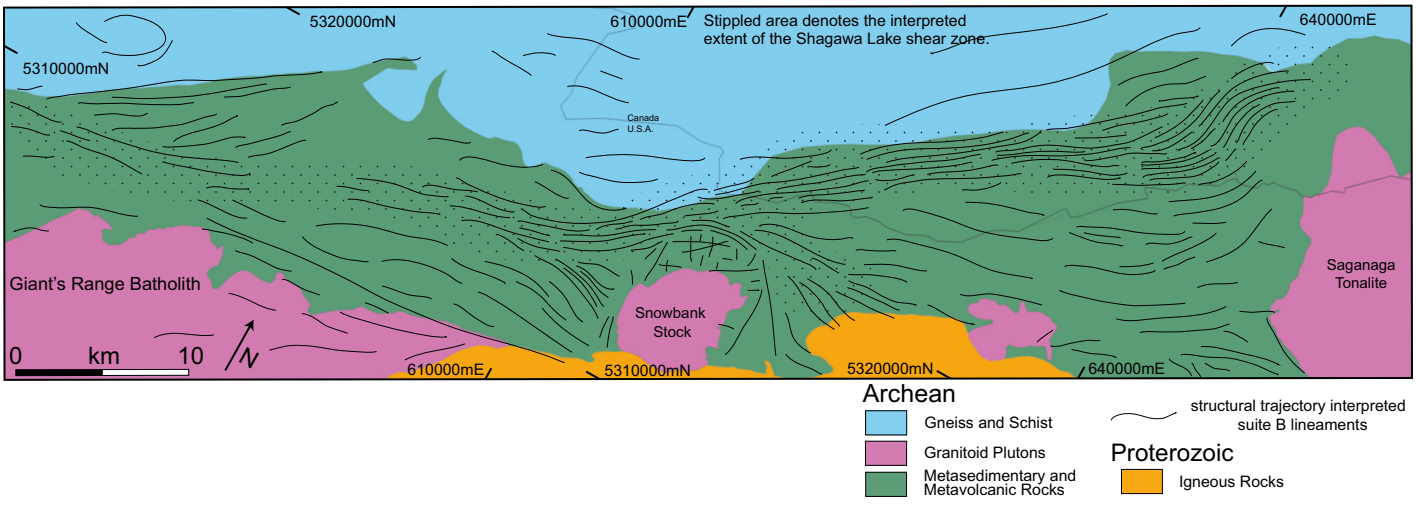

Figure 11. Simplified geologic map of the study area showing tectonic fabric interpreted from the suite B lineament fabric. Note the relative spacing of the tectonic fabric. Stipple marks areas of closely spaced, parallel lines that define a curvilinear zone (shear zone?) across the map area. The tectonic fabric diverges around granitoid plutons within the metasedimentary and metavolcanic sequence. Coordinate system UTM Zone 15, NAD 1983.

The techniques outlined herein can be applied to other areas of poorly exposed continentally glaciated terrane. Relatively large areas of bedrock with little to no sediment cover are necessary for Lidar altimetry to be applicable, because sediment can obscure bedrock lineaments. An important aspect of this study is that the erosion processes of glaciation and frost wedging do not allow the formation of microtopography; therefore construction of detailed structural maps (i.e., Pavlis and Bruhn, 2011) is difficult to impossible. Geologic setting, structural style, and erosion history directly control the topographic expression of the tectonic fabric, and different areas may preserve tectonic fabric at different scales. Our analysis shows that Lidar altimetry can be used to map regional tectonic fabric; researchers that use Lidar altimetry to analyze glaciated terrain should give careful consideration to geologic setting, structural style, and erosion history.

ACKNOWLEDGMENTS

Funding for this study provided by the McKnight Foundation (funds awarded to Vicki Hansen), the University of Minnesota Duluth Department of Geological Sciences, the Precambrian Research Center, the Institute on Lake Superior Geology, and the Harry and Margret Walker Foundation. Thanks to the National Forest Service and Ontario Parks Service for providing access to the Boundary Waters Canoe Area Wilderness and Quetico Provincial Park.

REFERENCES CITED

Bauer, R.L., and Bidwell, M.E., 1990, Contrasts in the response to dextral transpression across the Quetico-Wawa subprovince boundary in northeastern Minnesota: Canadian Journal of Earth Sciences, v. 27, p. 1521–1535, doi:10.1139/e90-162.

Bedard, J.H., Brouillette, P., Madore, L., and Berclaz, A., 2003, Archean cratonization and deformation in the northern Superior Province, Canada: An evaluation of plate tectonic versus vertical tectonic models: Precambrian Research, v. 127, p. 61–87, doi:10.1016/S0301-9268(03)00181-5.

Card, K.D., 1990, A review of the Superior Province of the Canadian Shield, a product of Archean accretion: Precambrian Research, v. 48, p. 99–156, doi:10.1016/0301-9268(90)90059-Y.

Chardon, D., Peucat, J., Jayananda, M., Choukroune, P., and Fanning, C.M., 2002, Archean granite-greenstone tectonics at Kolar (South India): Interplay of diapirism and bulk inhomogeneous contraction during juvenile magmatic accretion: Tectonics, v. 21, no. 3, p. 7-1–7-17, doi:10.1029/2001TC901032.

Chardon, D., Jayananda, M., and Chetty, T.R.K., 2008, Precambrian continental strain and shear zone patterns: South Indian case: Journal of Geophysical Research, v. 113, doi:10.1029/2007JB005299.

Chardon, D., Gapais, D., and Cagnard, F., 2009, Flow of ultra-hot orogens: A view from the Precambrian, clues for the Phanerozoic: Tectonophysics, v. 477, p. 105–118, doi:10.1016/j.tecto.2009.03.008.

Collins, B.C., and Sitar, N., 2008, Processes of costal bluff erosion in weakly lithified sands, Pacifica, California, USA: Geomorphology, v. 97, p. 483–501, doi:10.1016/j.geomorph.2007.09.004.

Erickson, E., 2008, Structural and kinematic analysis of the Shagawa Lake shear zone, Superior Province, northeastern Minnesota [M.S. thesis]: Duluth, University of Minnesota, 75 p.

Erickson, E., 2010, Structural and kinematic analysis of the Shagawa Lake shear zone, Superior Province, northern Minnesota: Implications for the role of vertical versus horizontal tectonics in the Archean: Canadian Journal of Earth Sciences, v. 47, p. 1463–1479, doi:10.1139/E10-054.

Goodman, S., 2008, Structural and kinematic analysis of the Kawishiwi Shear Zone, Superior Province [M.S. thesis]: Duluth, University of Minnesota, 164 p.

Gruner, J.W., 1941, Structural geology of the Knife Lake area of northeastern Minnesota: Geological Society of America Bulletin, v. 52, p. 1577–1642, doi:10.1130/GSAB-52-1577.

Haugerud, R.A., Harding, D.J., Johnson, S.Y., Harless, J.L., Weaver, C.S., and Sherrod, B.L., 2003, High-resolution topography of Puget Lowland, Washington—A bonanza for Earth science: GSA Today, v. 13, no. 6, p. 4–10, doi:10.1130/1052-5173(2003)13<0004:HLTOTP>2.0.CO;2.

Henderson, D.B., Ferrill, D.A., and Clarke, K.C., 1996, Mapping geological faults using image processing techniques applied to hill-shade digital elevation models: Proceedings of the IEEE Southwest Symposium on Image Analysis and Interpretation, p. 240–245.

Hobbs, H.C., and Goebel, J.E., 1982, Geologic map of Minnesota, Quaternary geology: Minnesota Geological Survey State Map Series S-01, scale 1:500,000, http://hdl.handle.net/11299/60085.

Jirsa, M.A., and Miller, J.D., Jr., 2004, Bedrock geology of the Ely and Basswood quadrangles, northeast Minnesota: Minnesota Geological Survey Map M-148, scale 1:100,000, ftp://mgssun6.mngs.umn.edu/map_catalog/pdf/umn22562.pdf.

Jirsa, M.A., Boerboom, T.J., Chandler, V.W., Mossler, J.H., Runkel, A.C., and Setterholm, D.R., 2011, Geologic map of Minnesota—Bedrock geology: Minnesota Geological Survey State Map Series S-21, scale 1:500,000, http://hdl.handle.net/11299/101466.

McNab, W.H. and Avers, P.E., compilers, 1994, Ecological subregions of the United States: Section descriptions: Washington, D.C., U.S. Department of Agriculture, Forest Service, Administrative Publication WO-WSA-5, 267 p.

Mulvey, L., Ross, C., Zeitler, J., Pendleton, M., McCarthy, A., Copp, L., Nowak, R., Hudak, G., Peterson, D., 2009, Bedrock geologic map of the Disappointment Lake area, Lake County, northeastern Minnesota: University of Minnesota Duluth Precambrian Research Center Map Series PRC/MAP-2009-02, scale 10,000.

Notebaert, B., Verstraeten, G., Govers, G., and Poesen, J., 2009, Qualitative and quantitative applications of LiDAR imagery in fluvial geomorphology: Earth Surface Processes and Landforms, v. 34, p. 217–231, doi:10.1002/esp.1705.

Pavlis, T.L., and Bruhn, R.L., 2011, Application of LIDAR to resolving bedrock structure in areas of poor exposure: An example from the STEEP study area, southern Alaska: Geological Society of America Bulletin, v. 123, p. 206–217, doi:10.1130/B30132.1.

Roering, J.J., 2008, How well can hill-slope evolution models explain topography? Simulating soil transport and production with high-resolution data: Geological Society of America Bulletin, v. 120, p. 1248–1262, doi:10.1130/B26283.1.

Sharp, R.P., 1953, Glacial features of Cook County, Minnesota: American Journal of Science, v. 251, p. 855–883, doi:10.2475/ajs.251.12.855.

Sims, P.K., 1976, Early Precambrian tectonic-igneous evolution in the Vermillion district, northeastern Minnesota: Geological Society of America Bulletin, v. 87, p. 379–389, doi:10.1130/0016-7606(1976)87<379:EPTEIT>2.0.CO;2.

Wallace, J., Morris, B., and Howarth, P., 2006, Identifying structural trend with fractal dimension and topography: Geology, v. 34, p. 901–904, doi:10.1130/G22632A.1.

Wolf, D.E., 2006, The Burntside Lake and Shagawa/Knife Lake shear zones: Deformation kinematics, geochemistry and geochronology; Wawa Subprovince, Ontario, Canada [M.S. thesis]: Pullman, Washington State University, 113 p.

Zhou, Q., 1992, Relief shading using digital elevation models: Computers & Geosciences, v. 18, p. 1035–1045, doi:10.1016/0098-3004(92)90019-N.